In Situ Production of Biofunctionalized Few-Layer Defect-Free Microsheets of Graphene

*Alfredo M. Gravagnuolo, Eden Morales-Narváez, Sara Longobardi, Everson T. da Silva, Paola Giardina, and Arben Merkoçi**

Biological interfacing of graphene has become crucial to improve its biocompatibility, dispersability, and selectivity. However, biofunctionalization of graphene without yielding defects in its sp^2-carbon lattice is a major challenge. Here, a process is set out for biofunctionalized defect-free graphene synthesis through the liquid phase ultrasonic exfoliation of raw graphitic material assisted by the self-assembling fungal hydrophobin Vmh2. This protein (extracted from the edible fungus *Pleurotus ostreatus*) is endowed with peculiar physicochemical properties, exceptional stability, and versatility. The unique properties of Vmh2 and, above all, its superior hydrophobicity, and stability allow to obtain a highly concentrated (≈440–510 μg mL^{-1}) and stable exfoliated material (ζ-potential, +40/+70 mV). In addition controlled centrifugation enables the selection of biofunctionalized few-layer defect-free micrographene flakes, as assessed by Raman spectroscopy, atomic force microscopy, scanning electron microscopy, and electrophoretic mobility. This biofunctionalized product represents a high value added material for the emerging applications of graphene in the biotechnological field such as sensing, nanomedicine, and bioelectronics technologies.

1. Introduction

Due to its extraordinary structure and fascinating properties, graphene is definitely the most studied nanomaterial.[1] Being the thinnest object ever known, graphene is a single layer of carbon atoms patterned in a 2D honeycomb network.[2] As the fundamental building block of carbon allotropes, it exhibits unparalleled properties such as high planar surface (≈2630 m^2 g^{-1}),[3] superlative mechanical strength (Young's modulus, ≈1100 GPa),[4] remarkable thermal[5] and electrical conductivity[6] (5000 W m^{-1} K^{-1} and 1738 S m^{-1}, respectively), high absorption of incident white light (2.3%, in spite of its thickness),[7] highly efficient fluorescence quenching capabilities,[8] and impermeability to standard gases.[9] Consequently, graphene can be integrated as the core of cutting-edge technologies and devices related to photonics, electronics, composite materials, sensors, environment, energy, biotechnology, and biomedicine.[10–13]

Since the groundbreaking discovery of the surprising properties of graphene,[14] the industrial and scientific communities have focused their attention on the development of new graphene synthesis methods enabling a variety of options in terms of oxidation grade, number of layers, edge and basal defects, lateral size, quality, and cost for any particular application.[10,15,16] According to the literature,[10,15] the most relevant routes for graphene generation are the chemical vapor deposition, epitaxial growth, mechanical cleavage, wet chemical synthesis, and exfoliation of graphite.[17,18]

Generally, liquid-phase exfoliation of graphite entails the use of ultrasonication as a key method which promotes the generation of laminated material that is subsequently bound to aggregate due to the lack of hydrophilic groups onto the exfoliated material. In fact, re/aggregation is one of the main challenges to address during the exfoliation procedure and the stabilization of solvent-dispersed graphene flakes.[18] However, re/aggregation is typically minimized by using organic solvents with suitable characteristics[19] or surfactant–water solutions.[20,21]

Biological interfacing of graphene has become crucial to improve its biocompatibility,[22] dispersibility, and selectivity toward various applications in the biotechnological and biomedical fields.[23–25] However, since chemical functionalization of graphene is generally known to sensitively disrupt its electronic structure,[26] the biofunctionalization of graphene without triggering defects, e.g., disrupting the sp^2-carbon lattice by introducing oxygen-containing groups, is a major challenge. Although graphene modification and biofunctionalization are under active research,[23] the in situ production of biofunctionalized defect-free graphene has been little explored.

Because of their huge range of functions and high responsiveness to a variety of stimuli, proteins are suitable candidates for bioconjugation of nanomaterials for biomedical

A. M. Gravagnuolo, Dr. E. Morales-Narváez, E. T. da Silva, Prof. A. Merkoçi
ICN2 – Catalan Institute of Nanoscience and Nanotechnology
08193 Barcelona, Spain
E-mail: arben.merkoci@icn.cat
A. M. Gravagnuolo, Dr. S. Longobardi, Prof. P. Giardina
Department of Chemical Sciences
University of Naples "Federico II,"
80126 Naples, Italy
Prof. A. Merkoçi
ICREA – Catalan Institution for Research and Advanced Studies
08010 Barcelona, Spain

DOI: 10.1002/adfm.201500016

applications. Protein binding onto pristine carbon lattice is strongly driven by hydrophobic interactions.[27] Besides hydropathicity character of amino acid residues, 3D protein structure also plays a key role in their adsorption onto graphene-based materials (GBMs) and functionality of the resulting bioconjugates. For instance, proteins prone to form amyloid structures strongly interact with carbon nanomaterials, forming bioinspired hybrid materials which show special properties and biodegradability.[28–30]

The use of amphiphilic proteins called hydrophobins from fungal sources has been reported to enable the coating of a wide variety of materials included carbon based materials.[31–34] Hydrophobins are small surface active proteins which play special roles at some stages in the growth and the development of filamentous fungi,[35] being able to self-assemble at hydrophilic–hydrophobic interface to form amphiphilic (mono) layers. Conventional soluble proteins confine hydrophobic residues in the core of the molecular structure and expose the hydrophilic ones to the solvent to reach a minimum of energy in aqueous environment. Conversely, the Janus-faced character of hydrophobins is due to the clustering of hydrophobic residues on one side of the protein surface maximizing the area of interaction with hydrophobic materials. Consequently, these peculiar proteins can tune the wettability of surfaces and improve their properties for biomedical applications such as sensing and drug delivery.[36–40] Moreover, the hydrophobin coating can confer special properties, i.e., prevention of human immune response,[41] specific functionalities trough protein engineering,[32] or molecular adsorption.[42]

The hydrophobin family is split in two classes on the basis of their structure and function;[35] Class I hydrophobins have natural propensity to self-assemble into remarkably stable amyloid-like nanostructures also known as rodlets, which can only be solubilzed in harsh acids.[43–47] Despite the superior stability of coating by Class I hydrophobins, technologies based on their use have been less exploited with respect to the Class II, possibly because of their lower solubility and high propensity to self-assemble which cause several drawbacks in their handling.

Recently, Laaksonen et al. have demonstrated a one-step approach for the ultrasonic wave-based exfoliation and functionalization of layered carbon materials using Class II hydrophobins from the filamentous fungus *Trichoderma reesei*. According to the model proposed by Laaksonen and co-workers, self-assembling hydrophobins at solvent–carbon interface tune the surface energy of the 2D carbon lattice in a surfactant-like system, thus reducing the interlayer stacking which is the driving force opposing to micromechanical exfoliation.

Class I hydrophobin, Vmh2 from the edible white-rot fungus *Pleurotus ostreatus*, has been purified and extensively studied by our research group.[48,49] Solvent polarity, pH, temperature, and the presence of calcium ions trigger the protein transition across structural states. Vmh2 self-assembling into nanometric films has been explored[50,51] as well as its capability to recruit biomolecules, such as glucose or a variety of enzymes in their active form, onto the biohybrid surface.[42,52] Moreover, surface (silicon and steel) functionalization by Vmh2 has been demonstrated to leave unaltered the optical properties and to be effective in technological devices.[51,53,54]

Herein, we explore the ultrasonication-based production of biofunctionalized graphene using the Vmh2 hydrophobin. As depicted in **Figure 1**, we exfoliate a low-cost graphite source (graphite powder, Aldrich 332461) in ethanol–water media by a medium power (125 W, 20 kHz. Inbuilt power meter power output 19 W) tip sonicator. Controlled centrifugation (final steps at 620 and 2500 g) enables us to obtain suspensions of particles of controlled size. They are endowed with exceptional stability in liquid (ethanol–water) due to the hydrophobin coating. Since on one hand the number of graphene layers and their defects significantly modulate the succeeding transport properties,[55] and on the other hand the lateral dimension size controls the maximum dimension and degree of deformability of the material that are paramount parameters for biological interactions,[56,57] we systematically study the quality of the generated graphene sheets in terms of lateral dimension, number of layers per flakes, and defect characteristics. To this aim, we exploit recent advances in graphene Raman spectroscopy in terms of spectral analysis of GBMs[58] and study the self-assembled biohybrid structures by AFM, scanning electron microscopy (SEM) and electrokinetic analysis.

2. Results and Discussion

2.1. In Situ Exfoliation, Functionalization, and Stabilization of GBMs by Vmh2 Hydrophobin

Ultrasonication of graphite powder (1000 μg mL^{-1}) in Vmh2 hydrophobin solution (50–100 μg mL^{-1} in 60%, v/v, ethanol in water, 5 mL volume) resulted in dark and stable dispersions of carbon material, see **Figure 2**A,b. When micromechanical exfoliation was attempted in the absence of the surface active protein, flocculation and settling out occurred in 3 days owing to interlayer stacking of newly formed flakes, see Figure 2A,a. SEM imaging shed light on the starting material, crystallites of ≈1 mm lateral size (Figure 2B), and on the product of Vmh2 assisted exfoliation/stabilization, an heterogeneous mix of GBMs in terms of particles size (up to 2 μm) and shape, see Figure 2C.

Aiming at estimating the amount of GBMs attainable by the Vmh2-assisted exfoliation, the unexfoliated graphite was removed by gentle centrifugation, 40 min at 40 g, then, UV–vis measurements[20,32] indicated a concentration of ≈440–510 μg mL^{-1} of carbon dispersion. This value was one order of magnitude higher than that one previously reported by Laaksonen and co-workers using Class II hydrophobins. In addition, they have employed high-class graphitic sources (HOPG and Kish graphite, which are expensive when compared with graphite powder: Kish graphite ≈350 USD, 0.5 g; highly ordered pyrolytic graphite (HOPG) ≈200 USD, mosaic of 5 × 5 mm, thickness 2.0 mm; graphite powder, ≈72.8 USD, 2.5 kg) in 0.3–1 mL volumes of water solutions, obtaining a 25–40 μg mL^{-1} suspension of exfoliated material.[32] In spite of the considerable differences in the geometry of the proposed processes (see Table S1, Supporting Information), we believe that the unique properties of Vmh2 and, above all, its superior hydrophobicity and stability (as described below) play a significant role in such an advance.

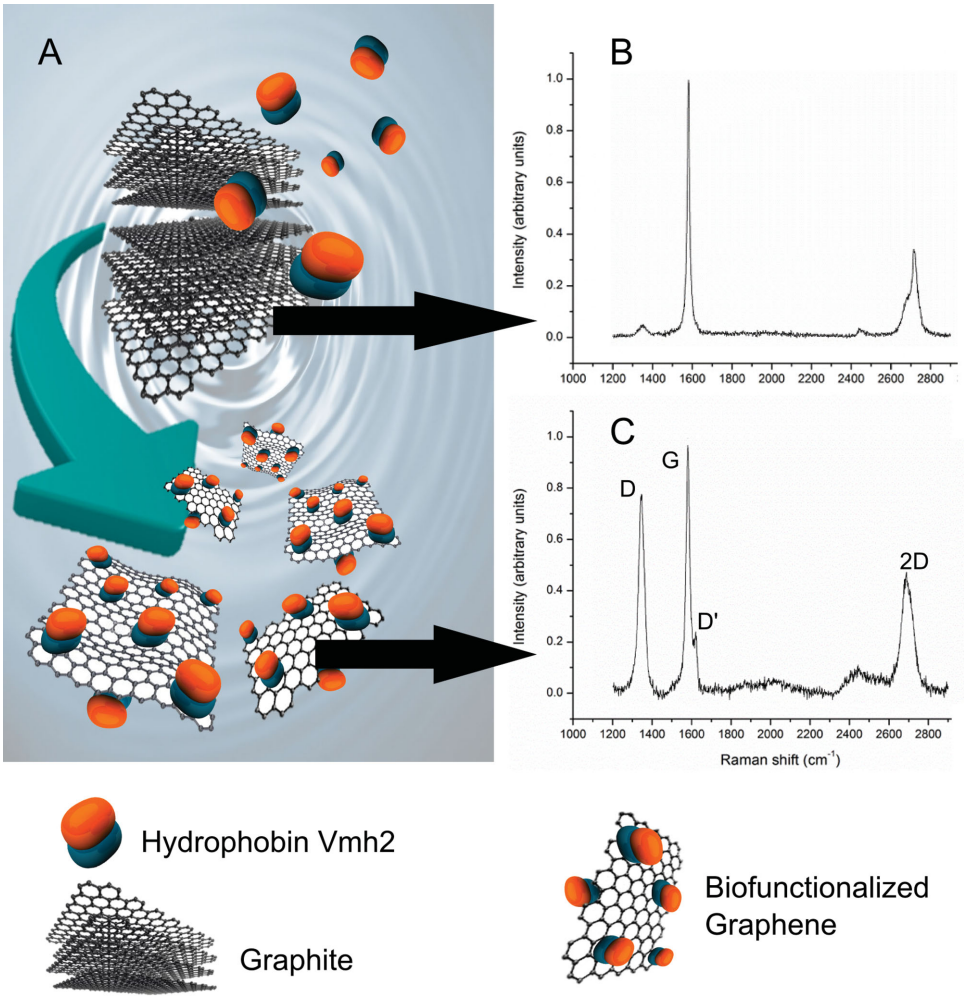

Figure 1. In situ generation of biofunctionalized graphene. A) Schematic representation of the process. Ultrasound waves are applied as a source of mechanical force that brakes and exfoliates the starting material (graphite). Subsequently, the hydrophobic region of the amphiphilic protein hydrophobin Vmh2 is spontaneously adsorbed onto the laminated material (which is also hydrophobic) stabilizing and functionalizing the exfoliated material. B) Raman spectra of the starting material (graphite crystallites). C) Raman spectra of the generated material (biofunctionalized few-layer graphene flake). Experimental conditions as given in the text.

Sequence analysis of hydrophobins and soluble standard proteins with different physicochemical and functional characteristics evidenced that (i) hydrophobins show major contribution of hydrophobic amino acids with respect to the other soluble proteins and (ii) Vmh2 is the most hydrophobic hydrophobin among those that have been used for the stabilization of nanomaterials to date (see Figure S1, Supporting Information). To give insight into its amphiphilic character, the sequence of Vmh2 was compared with that of hydrophobin HFBI used by Laaksonen and co-workers. Hydropathy analysis suggested that Vmh2 brings into play very extended hydrophobic patches that could strongly drive Vmh2 onto GBMs surface (see Figure S2, Supporting Information).

Usually stability to physical and chemical factors deeply limits the use of biological molecules in cutting-edge technology approaches. Irreversible conformational transitions commonly lead to loss of function and aggregation of proteins, often in a temperature dependent kinetics. In contrast, mature Vmh2 is a small (87 amino-acids) and compact protein, particularly resistant to chemical and physical treatments.[51] It is worth mentioning that partial protein unfolding has been reported to occur at 80 °C, however the protein refolds by lowering the temperature at 25 °C.[48] Moreover, batches of Vmh2 protein dissolved in 60 vol%. ethanol solution were soluble and functional at least 18 months at room temperature. This very stable state has been achieved by using a low polar solvent able to solvate the extended hydrophobic patches exposed on the surface of protein. Vmh2 protein showed extreme resistance also in our system, where intensive ultrasonication causes heating of the solution. Likewise, GBM dispersions were stable for at least 6 months at room temperature.

It should be remarked that Vmh2 was also able to stabilize carbon dispersions from different graphite sources by adding the protein either before (see Figure S3, left, Supporting Information) or after exfoliation. Vmh2-assisted ultrasonication of

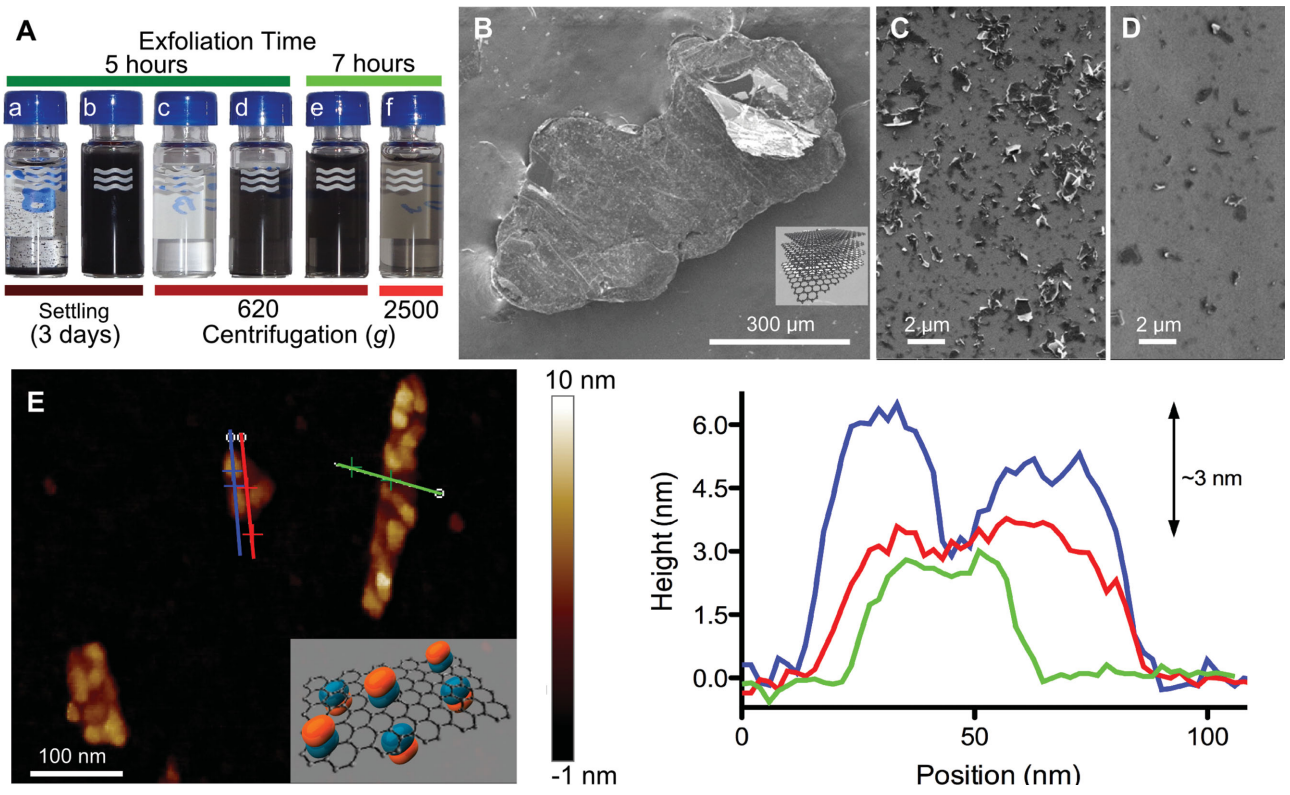

Figure 2. Production of Biofunctionalized Graphene. A) Samples of the dispersions obtained through a,c) liquid phase exfoliation in absence of Vmh2 and b,d,e,f) Vmh2 assisted exfoliation. B) SEM image of the starting material (graphite flake). C) SEM image of the dispersion shown in (A,b). D) SEM image of the dispersion displayed in (A,d). E, left) AFM analysis of biofunctionalized graphene obtained from the sample HC shown in (A,f). E, right) AFM profiles of two flakes showing the graphene–Vmh2 assembly. Experimental conditions as given in the text.

HOPG as well as addition of Vmh2 to a previously exfoliated HOPG or to a commercial GBM allowed the improvement of their dispersibility and their use for surface functionalization. Indeed, drop casting of the obtained dispersions resulted in a very homogenous coating of silicon chips upon solvent evaporation as shown by SEM imaging (see Figures S3, right, and S4, Supporting Information).

The use of smart and self-assembled materials inspired from nature whose properties are dependent on external chemical or physical stimuli is emerging in biomedical field.[59] The complex behavior of Vmh2 in ethanol/water solvents has been previously elucidated.[48] Its aggregation can be controlled by environmental factors such as solvent polarity, temperature, divalent cations, or base addition.[48] Interestingly, we observed that the biohybrid GBM obtained by Vmh2 assisted exfoliation was endowed with the self-assembling characteristics of the protein moiety which enabled analogous handling of the material morphology. As solvent polarity was increased, by adding water to the water/ethanol solution, the Vmh2 assisted exfoliated GBMs reached the liquid–air or liquid–solid interface forming a homogeneous film (see Figure S5 and the video, Supporting Information). Moreover, ammonia additions triggered the formation of Vmh2–GBM coaggregated in solution, see Figure S5, right, Supporting Information. All these results suggest the wide flexibility of this technology in adding value to carbon materials for an easy handling and applicability.

2.2. Production of Biofunctionalized GBMs

We aim at contributing a cost-effective scalable process for the production of biofunctionalized graphene with well-defined characteristics. We optimized the process parameters to obtain the maximum yield (≈45%–50%) and production rate (≈13–15 µg mL^{-1} h^{-1}): exfoliation time (5–7 h), amount of starting material (≈1 mg mL^{-1}), carbon/protein ratio (w/w 20:1), and Vmh2 concentration (50–100 µg mL^{-1}). Figure S6, Supporting Information, summarizes the most relevant parameters of the optimization process. Selection of GBMs classes on the base of particles size is easily and reliably achievable by controlled centrifugation.[58,60] In particular, after removal of unexfoliated material (40 min at 40 g), consecutive 40 min centrifugations at increased centrifugal force were tested. Since it has been reported that the average number of monolayers per flakes reaches a minimum at ≈2500 g,[58] we characterized the dispersions obtained after medium (620 g), and hard centrifugation (2500 g) steps, named MC and HC samples, respectively. As expected, the applied centrifugal force dramatically influenced the GBMs yield in solution (see Figure 2A). SEM imaging proved an evident reduction of graphite microplatelets and an improvement of homogeneity using both MC and HC (see Figure 2D showing SEM image of MC).

We also characterized the electrokinetic behavior of both MC and HC (see Figure S7, Supporting Information). Pure Vmh2 protein in an electric field migrated toward the

negative electrode in solution showing that the protein held a net positive charge, with an electrophoretic mobility (U_e) of 0.55 ± 0.06 μm s^{-1} cm V^{-1} (mean and standard error calculated on 10 sets of measurements). Moreover this value increased in the presence of exfoliated graphene up to 0.71 ± 0.03 μm s^{-1} cm V^{-1} in the case of HC sample and up to 0.80 ± 0.03 μm s^{-1} cm V^{-1} in the case of MC sample. Since the graphene surface is highly nonpolar this change suggested that new species were assembled upon mixing of protein and GBMs through the adsorption of charged Vmh2 molecules onto the surface of carbon particles. The new molecular assemblies showed increased electrokinetic properties probably due to increased surface charge density and to the very unique solvent–sample relationship. We concluded that the interaction between graphene and the amphiphilic protein Vmh2 resulted in the formation of biohybrid assemblies endowed with a positive surface charge density.

The electrostatic repulsion generated by the protein coating could also explain the stabilization of graphene by Vmh2. Indeed, the estimation of ζ-potential from electrophoretic mobility could assess the stability of the graphene dispersion through a model in which the protein act as a surfactant.[20,21] We could estimate the ζ-potential of Vmh2-coated graphene flakes by the Henry equation (see the Experimental Section). Considering the Huckel and Smoluchowski limits of the Henry function, we calculated both the lower and upper bounds of ζ-potential. Values ranged between +40 and +70 mV for Vmh2 assisted exfoliated samples, classifying the biofunctionalized graphene as highly stable.[20]

Evidences of the Vmh2 coating on carbon particles were found out through AFM analysis of HC sample (see Figure 2E). On the basis of the height of the assembly in the AFM profiles and the expected diameter of a hydrophobin molecule (≈3 nm) we could assess that Vmh2 formed a discontinuous, one molecule thick coating. However, since the resolution on the *XY* plane was quite low because of the so-called tip effect, the observed islands could be made of isolated Vmh2 monomers and/or oligomers.

In order to estimate the number of graphene layers per flake, as described below, we used Raman spectroscopy, since AFM analysis provides the top profile of the flakes while the structure of the lower layers is hidden.

2.3. Raman Spectroscopy Characterization and Classification of Biofunctionalized Graphene

Currently, health risk associated to GBMs is under debate.[57,61,62] Establishing the characteristics of the biofunctional graphene is essential to define the structure–safety relationship which is a future challenge concerning the use of graphene materials in biomedical applications. In order to avoid ambiguities in terms of characteristics of GBMs a classification approach has been recently proposed.[57,63] Such a nomenclature is based on the specification of the three most significant characteristics of the GBMs which modulate the chemical, physical, and biological properties: number of graphene layers (N_G); lateral size (*L*, being rectangular-like structures, it generally refers to the maximum lateral dimension of the inspected flake); and defect type. Latest advances in Raman spectroscopy analysis have enabled a simple and consistent estimation of all these parameters.

First, to investigate on the most important parameter, N_G, we fully capitalized on the Raman spectroscopy analysis recently proposed by Paton et al.[58] Characteristics of the classic 2D band are associated with the stacking of carbon layers in GBM. The authors have developed a metric on the base of the consideration that the spectral intensity at the wavenumber corresponding to the 2D peak of graphite (ω_p) and its shoulder ($\omega_s = \omega_p - 30$ cm^{-1}) is strictly correlated to N_G, see details in the Experimental Section. The result of the Raman analysis on the graphite spectrum (see **Figure 3**F) compared to those of some Vmh2 coated flakes demonstrated that few-layer graphene (2/5 N_G) was produced (see Figure 3A–E).

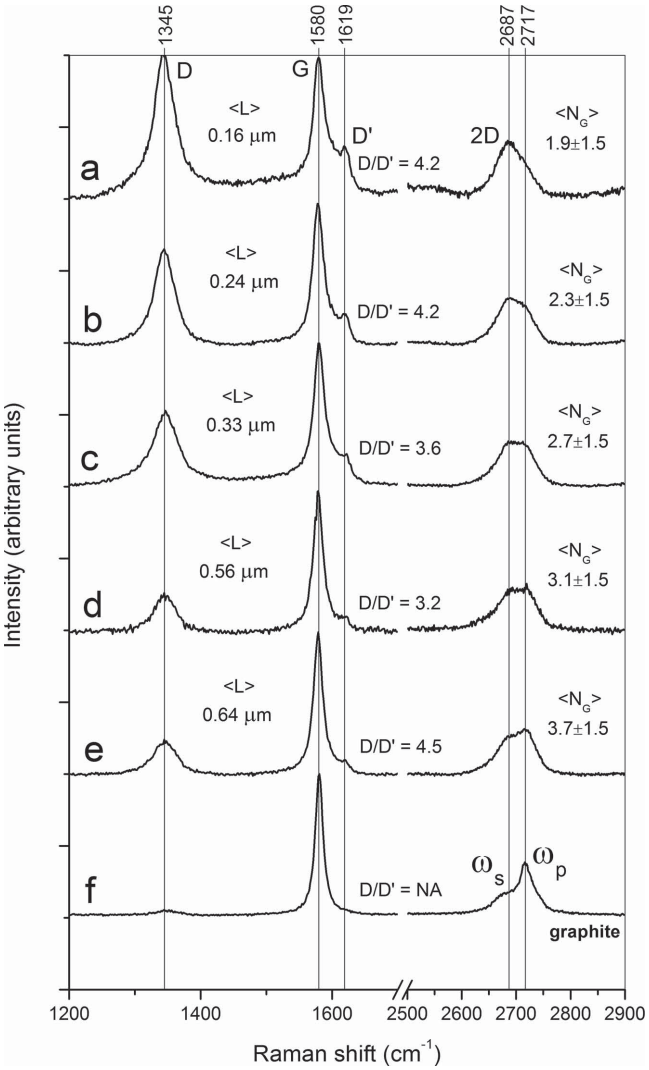

Figure 3. A–E) Quality assessment by Raman spectroscopy analysis of a,b,c,d,e) biofunctionalized flakes of increasing sizes (from HC sample) and of F) graphite, i.e., the starting material, indicating the wavenumbers corresponding to *D*, *G*, *D'*, 2D peak of graphite (ω_p) and its shoulder ($\omega_s = \omega_p - 30$ cm^{-1}) and the estimated lateral dimension ($\langle L \rangle$), *D*/*D'* ratio obtained by fitting and estimated number of graphene layers ($\langle N_G \rangle$). Experimental conditions as given in the text.

Second, to check if the proposed process introduces damages, in the basal plane of graphene we studied defect-activated Raman signals, D (≈1345 cm^{-1}) and the D' (≈1620 cm^{-1}). Since the reduction of the flakes size determines an increase of the total boundaries, an intrinsic contribution to the D' band arises from edge type defects in exfoliated samples. Moreover graphite sources of different qualities could contain natural defects in the basal plane, i.e., sp3 and vacancy-like defects. Herein, the D band in spectra of crystallites we used for the synthesis of graphene was scarcely represented, so assessing the good quality of the starting material (Figure 3F). On the other hand, intense D signals were detected in the exfoliated flakes (Figure 3A–E). To check if Vmh2 based exfoliation introduced damages in basal plane of graphene, we characterized the defect types analyzing the intensity ratio of the D and D' peaks through Lorentzian fitting.[64] According to Eckmann et al., values of $D/D' \approx 13$ indicated sp^3 defects, $D/D' \approx 7$ vacancy defects, and $D/D' \approx 3.5$ edge defects. The latter value has been revised by Paton et al. to include the error analysis: $3 \geq D/D'_{\text{edge defects}} \geq 4.5$.[58] All the calculated values of D/D' (Figure 3A–E) in our samples lied in the range indicated for edge type defects. It is worth noting that we set up the maximum ratio of ultrasonication power to reaction volume and the associated solvent heating was attenuated by ice bath cooling. Nevertheless, according to the data acquired experimentally using Raman, defects cannot be ascribed to the basal plane; hence we can conclude that no oxidation of graphene occurred in the course of exfoliation. This is likely due to the essential characteristics of the ultrawave exfoliation technique and to the protection of the Vmh2 coating against surface oxidation.

Third, once demonstrated that only edge type defects were introduced during the exfoliation, Raman spectroscopy analysis enabled the estimation of graphene lateral size ($\langle L \rangle$) through a metric based on the intensity ratio of the D and G peaks (D/G),[58,65,66] (see details in the Experimental Section). Spectra (Figure 3A–E) evidenced that the analyzed flakes were micrometer-sized. Interestingly, a positive correlation between $\langle N_G \rangle$ and $\langle L \rangle$ was observed, although the two properties were estimated by the analysis of separate signals.

Finally, in order to unequivocally assess the quality of material, we performed a complete Raman analysis on 40 biofunctionalized flakes (see **Figure 4**), 16 from MC and 24 from HC sample. The $\langle N_G \rangle$ in both the samples laid in the 2/5 range, with an average value of 3.8 ± 0.4 (standard error) layers in MC and of 2.9 ± 0.3 layers in HC. These data allowed the classification of both materials as few-layer graphene.[63] Furthermore, on the base of the average lateral dimension, 1.0 ± 0.1 µm for MC, 0.49 ± 0.06 µm for HC, we classified the material as micrographene. Moreover, the statistical distribution of $\langle N_G \rangle$ and $\langle L \rangle$ data from all the 40 flakes confirmed their positive correlation (see Figure 4A). Then, the D/D' ratio data distribution definitely characterized the biofunctionalized graphene as defect free, hence lacking in functional groups of oxygen covalently bound to the basal plane (see Figure 4B). All these results are summarized in **Table 1** putting into context both MC and HC materials as biofunctionalized defect-free few-layer micrographene.

3. Conclusion

We have demonstrated a method for the production of biofunctionalized defect-free GBMs by using a unique fungal protein, the hydrophobin Vmh2 extracted from the edible fungus *P. ostreatus*. Due to superior hydrophobicity and stability of Vmh2, we have obtained high concentration of GBMs (≈440/510 µg mL^{-1}) upon Vmh2 assisted exfoliation of raw graphitic material. Furthermore, we have proved through an accurate characterization that controlled centrifugation enables the selection of very stable (>8 months, ζ-potential +40/+70 mV), few-layer (<5 layers), and defect-free graphene (≈90/100 µg mL^{-1}) with an average lateral dimension of 1.0 ± 0.1 µm. Interestingly, the strong interplay between protein and graphene allows also the formation of either thin films on a silicon by the drop casting method or self-assembled biohybrid structures in solution by modulating the environmental conditions. As a potentially scalable approach, this method could enable massive production of biofunctionalized graphene, which could be a valuable material for the upcoming

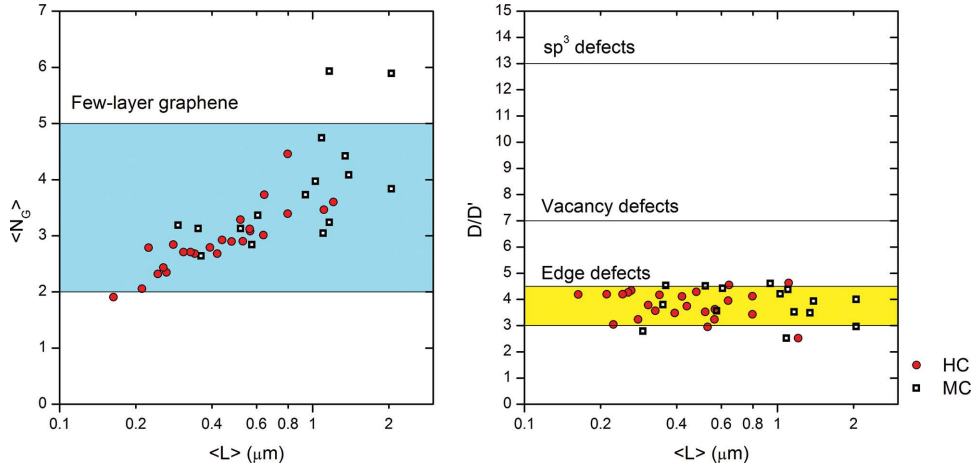

Figure 4. Statistical distribution of (left) the $\langle N_G \rangle$ and (right) the D/D' ratio, in MC and HC samples used for GBM classification. Experimental conditions as given in the text.

diffusion of new nanobiotechnologies in the global biomedical market.[10,11]

4. Experimental Section

Vmh2 Extraction from P. Ostreatus Mycelia: White-rot fungus, *P. ostreatus* (Jacq.: Fr.) Kummer (type: Florida; ATCC No. MYA-2306) was maintained at 4 °C through periodic transfer on potato dextrose agar (Difco) plates in the presence of 0.5% yeast extract. Mycelia were inoculated in 1 L flasks containing 500 mL of potato-dextrose broth (24 g L^{-1}) supplemented with 0.5% yeast extract, grown at 28 °C in shaken mode (150 rpm). After 10 days of fungal growth, mycelia were separated by filtration through gauze, treated twice with 2% sodium dodecyl sulfate (SDS) in a boiling water bath for 10 min, washed several times with water and once with 60% ethanol to completely remove the detergent. The residue was dried under nitrogen, grinded and treated with 100% trifluoroacetic acid (TFA) in a water bath sonicator (Elmasonic S30, Elma) for 30 min, and centrifuged (10 min at 3200 g). The supernatant was dried, and then lipids were extracted in a mixture of water–methanol–chloroform 2:2:1 v/v (5 min in bath sonicator). After centrifugation, proteins appeared as a solid aggregate at the interface between the water–methanol and the chloroform phases. They were recovered by liquid phase removal. The aggregated protein was dried, treated with TFA for 30 min in bath sonicator, redried, and dissolved in 80% ethanol. The sample was centrifuged (90 min at 12 000 g) and ethanol was removed from the supernatant under vacuum at 40 °C using rotavapor and the material was freeze-dried, treated with TFA as abovedescribed, and redissolved in 60% ethanol.

Exfoliation and Stabilization Process: Graphite powder (Aldrich, 332461, mesh number of grains +100, >75%) is exfoliated in batches of 5 mL of 60%, v/v, ethanol in MilliQ water (in 10 mL flasks), 17–200 μg mL^{-1} Vmh2, using a medium power tip sonicator (Q125 Sonicator, QSonica, 125 W, 20 kHz, inbuilt power meter power output, 19 W) and cooling the system in an ice bath. Concentration of dispersions is estimated by UV–vis spectroscopy. Absorption spectra are acquired on a UV–vis spectrophotometer SpectraMax M2e using a quartz cell 1 cm optics. Upon the subtraction of the solvent spectrum, we use the absorption coefficient value at 660 nm (1390 g L cm^{-1}) previously established by Lotya et. al.[20] in a surfactant exfoliation process and also used in the hydrophobin-assisted exfoliation reported by Laaksonen et al.[32] Controlled centrifugation is performed using a Sigma 2–16PK FIsher Bioblock Scientific centrifuge (rotor 12072 418/H) in 15 mL tubes. HOPG (1000 μg mL^{-1}) is exfoliated as previously described, for 2 h in presence of Vmh2 protein (50 μg mL^{-1}) and left to settling for 3 days to remove the unexfoliated material. Alternatively, HOPG is biofunctionalized immediately after ultrasonication by mixing with a Vmh2 solution and treating 10 min in a bath sonicator (Fisherbrand, FB15051). A commercial GBM (Haydale, GNPs-O2) is resuspended in 6/4 (v/v) ethanol/MilliQ water solution, Vmh2 (50–400 μg mL^{-1}), sonicated 10 min in bath sonicator and used.

Characterization: Scanning Electron Microscopy (SEM) images are acquired using a FEI Quanta 650 FEG ESEM, 2 kV microscope upon drop casting 3 μL of solution on a silicon chip. AFM measurements are performed on mica using a Nanoscope V Multimode8 AFM (Bruker, Germany) and Si cantilevers (SNL model, k:0.3N/m, Bruker). The scanning probe microscopy is carried out at a scan rate of 1 Hz and 512 × 512 pixel. Electrokinetic analysis is carried out in folded capillary cells using a Malvern Zetasizer Nano-ZS system equipped with a 633 nm He–Ne laser. The instrument uses a combination of electrophoresis and laser Doppler velocimetry techniques to measure the electrophoretic mobility (U_e). All measurements are conducted at 25 °C. ζ-potential is estimated using the Henry equation

$$U_e = \frac{2}{3}\frac{\varepsilon\zeta}{\eta} f(ka) \tag{1}$$

where U_e is the electrophoretic mobility, ε and η are the dielectric constant and the viscosity of the solvent respectively, ζ is the ζ-potential, and $f(ka)$ is the Henry function. Considering that the approximations for Henry function range between the Huckel and Smoluchowski limits, 1/1.5, we estimate the upper and lower bound for the ζ-potential. Raman spectra are acquired using a Horiba Jobin Yvon LabRAM HR 800, 800 mm focal length, 100× objective, excitation wavelength 532 nm. Exfoliated samples are drop casted for analysis on corning microscope glass slides (Aldrich, CLS294775×25), laser is focused on samples and multiple spectra are accumulated. For estimation of N_G and L we use the Raman metrics reported by Paton et al.[58]

$$\langle N_G\rangle \begin{cases} N_G = 10^{0.84M+0.45M^2} \\ M = \dfrac{I_{G'ene}\left(\omega=\omega_{p,G'ite}\right)/I_{G'ene}\left(\omega=\omega_{s,G'ite}\right)}{I_{G'}\left(\omega=\omega_{p,G'ite}\right)/I_{G'}\left(\omega=\omega_{s,G'ite}\right)} \end{cases} \tag{2}$$

$$\langle L\rangle \begin{cases} L = \dfrac{k}{(D/G)_{G'ene} - (D/G)_{G'ite}} \\ (D/G)_{G'ite} = 0.034 \\ k = 0.17 \end{cases} \tag{3}$$

Table 1. Summary of MC and HC samples characteristics.

Graphene property	Type of analysis	MC	HC
Average $\langle N_G\rangle$	Raman; 2D based metric[60]	3.8 ± 0.4 layers	2.9 ± 0.3 layers
Average $\langle L\rangle$	Raman; D/G based metric[60]	1.0 ± 0.1 μm	0.49 ± 0.06 μm
Defect type/oxidation	Raman D/D' based classification[60,66]	D/D' 3.8 ± 0.2	D/D' 3.8 ± 0.1
		Edge type defects	Edge type defects
		Not oxidized	Not oxidized
Biofunctionalization	AFM	Vmh2 monolayer	Vmh2 monolayer
	Electrophoretic mobility	Positive surface charge density	Positive surface charge density
Stability	Time	>8 months	>8 months
	ζ-potential[22]	+40/+70 mV	+40/+70 mV
Concentration	UV–vis spectroscopy[22,34]	90/100 μg mL^{-1}	20/30 μg mL^{-1}

Analysis of MC and HC performed on 16 and 24 individual flakes, respectively, and reported for each parameter as mean ± standard error. The standard error of ⟨NG⟩ was calculated on the base of a fix error of ±1.5 on the single measurements.

where $I_{G'ite}(\omega = \omega_{p,G'ite})$ is the intensity of graphite 2D peak, $I_{G'ite}(\omega = \omega_{s,G'ite})$ is the intensity of graphite 2D shoulder measured at –30 cm^{-1} in respect to 2D peak (see Figure 3), $I_{G'ene}(\omega = \omega_{p,G'ite})$ is the intensity of graphene spectrum at the wavenumber corresponding to graphite 2D peak (2717 cm^{-1}), $I_{G'ene}(\omega = \omega_{s,G'ite})$ is the intensity of graphene spectrum at wavenumber corresponding to graphite 2D shoulder (1686 cm^{-1}), $(D/G)_{G'ite}$ is the value of D/G for graphite, and k is the slope that has been estimated by Paton et al. for the same graphitic material.

Supporting Information

Supporting Information is available from the Wiley Online Library or from the author.

Acknowledgment

A.M.G. and E.M.-N. contributed equally to this work. This work was supported by The European Commission Program, FP7-OCEAN (613844) and MINECO (Spain; BIO2013–49464-EXP and RTC-2014–2619–7); Ministero dell'Università e della Ricerca Scientifica (Italy)—Industrial Research Project PON01_01966 EnerbioChem, funded in the frame of Operative National Programme Research and Competitiveness 2007–2013 D. D. Prot. n. 01/Ric. 18.1.2010; P.O.R. Campania FSE 2007–2013, Project CREMe. ICN2 acknowledges support from the Severo Ochoa Program (MINECO, Grant SEV-2013–0295).

Received: January 2, 2015
Revised: March 4, 2015
Published online: March 30, 2015

[1] A. K. Geim, *Science* **2009**, *324*, 1530.
[2] A. K. Geim, K. S. Novoselov, *Nat. Mater.* **2007**, *6*, 183.
[3] M. D. Stoller, S. Park, Y. Zhu, J. An, R. S. Ruoff, *Nano Lett.* **2008**, *8*, 3498.
[4] C. Lee, X. Wei, J. W. Kysar, J. Hone, *Science* **2008**, *321*, 385.
[5] A. A. Balandin, S. Ghosh, W. Bao, I. Calizo, D. Teweldebrhan, F. Miao, C. N. Lau, *Nano Lett.* **2008**, *8*, 902.
[6] M. F. El-Kady, V. Strong, S. Dubin, R. B. Kaner, *Science* **2012**, *335*, 1326.
[7] R. R. Nair, P. Blake, A. N. Grigorenko, K. S. Novoselov, T. J. Booth, T. Stauber, N. M. R. Peres, A. K. Geim, *Science* **2008**, *320*, 1308.
[8] L. Gaudreau, K. J. Tielrooij, G. E. D. K. Prawiroatmodjo, J. Osmond, F. J. G. de Abajo, F. H. L. Koppens, *Nano Lett.* **2013**, *13*, 2030.
[9] J. S. Bunch, S. S. Verbridge, J. S. Alden, A. M. van der Zande, J. M. Parpia, H. G. Craighead, P. L. McEuen, *Nano Lett.* **2008**, *8*, 2458.
[10] A. C. Ferrari, F. Bonaccorso, V. Fal'ko, K. S. Novoselov, S. Roche, P. Bøggild, S. Borini, F. H. L. Koppens, V. Palermo, N. Pugno, J. A. Garrido, R. Sordan, A. Bianco, L. Ballerini, M. Prato, E. Lidorikis, J. Kivioja, C. Marinelli, T. Ryhänen, A. Morpurgo, J. N. Coleman, V. Nicolosi, L. Colombo, A. Fert, M. Garcia-Hernandez, A. Bachtold, G. F. Schneider, F. Guinea, C. Dekker, M. Barbone, Z. Sun, C. Galiotis, A. N. Grigorenko, G. Konstantatos, A. Kis, M. Katsnelson, L. Vandersypen, A. Loiseau, V. Morandi, D. Neumaier, E. Treossi, V. Pellegrini, M. Polini, A. Tredicucci, G. M. Williams, B. H. Hong, J.-H. Ahn, J. M. Kim, H. Zirath, B. J. van Wees, H. van der Zant, L. Occhipinti, A. Di Matteo, I. A. Kinloch, T. Seyller, E. Quesnel, X. Feng, K. Teo, N. Rupesinghe, P. Hakonen, S. R. T. Neil, Q. Tannock, T. Löfwander, J. Kinaret, A. C. Ferrari, *Nanoscale* **2015**, *7*, 4598.
[11] *Nat. Nanotechnol.* **2014**, *9*, 737.
[12] E. Morales-Narváez, A.-R. Hassan, A. Merkoçi, *Angew. Chem. Int. Ed.* **2013**, *52*, 13779.
[13] E. Morales-Narváez, A. Merkoçi, *Adv. Mater.* **2012**, *24*, 3298.
[14] K. S. Novoselov, A. K. Geim, S. V Morozov, D. Jiang, Y. Zhang, S. V Dubonos, I. V Grigorieva, A. A. Firsov, *Science* **2004**, *306*, 666.
[15] K. S. Novoselov, V. I. Fal[prime]ko, L. Colombo, P. R. Gellert, M. G. Schwab, K. Kim, *Nature* **2012**, *490*, 192.
[16] R. S. Edwards, K. S. Coleman, *Nanoscale* **2013**, *5*, 38.
[17] S. Eigler, A. Hirsch, *Angew. Chem. Int. Ed.* **2014**, *53*, 7720.
[18] S. Park, R. S. Ruoff, *Nat. Nanotechnol.* **2009**, *4*, 217.
[19] Y. Hernandez, M. Lotya, D. Rickard, S. D. Bergin, J. N. Coleman, *Langmuir* **2010**, *26*, 3208.
[20] M. Lotya, Y. Hernandez, P. J. King, R. J. Smith, V. Nicolosi, L. S. Karlsson, F. M. Blighe, S. De, Z. Wang, I. T. McGovern, G. S. Duesberg, J. N. Coleman, *J. Am. Chem. Soc.* **2009**, *131*, 3611.
[21] R. J. Smith, M. Lotya, J. N. Coleman, *New J. Phys.* **2010**, *12*, 125008.
[22] K. Yang, Y. Li, X. Tan, R. Peng, Z. Liu, *Small* **2013**, *9*, 1492.
[23] Y. Wang, Z. Li, J. Wang, J. Li, Y. Lin, *Trends Biotechnol.* **2011**, *29*, 205.
[24] C. Chung, Y.-K. Kim, D. Shin, S.-R. Ryoo, B. H. Hong, D.-H. Min, *Acc. Chem. Res.* **2013**, *46*, 2211.
[25] K. V. Krishna, C. Ménard-Moyon, S. Verma, A. Bianco, *Nanomedicine* **2013**, *8*, 1669.
[26] T. S. Sreeprasad, V. Berry, *Small* **2013**, *9*, 341.
[27] M. Calvaresi, F. Zerbetto, *Acc. Chem. Res.* **2013**, *46*, 2454.
[28] C. Li, R. Mezzenga, *Nanoscale* **2013**, *5*, 6207.
[29] M. I. Solar, M. J. Buehler, *Nat. Nanotechnol.* **2012**, *7*, 417.
[30] C. Li, J. Adamcik, R. Mezzenga, *Nat. Nanotechnol.* **2012**, *7*, 421.
[31] W. Yang, Q. Ren, Y.-N. Wu, V. K. Morris, A. a Rey, F. Braet, A. H. Kwan, M. Sunde, *Biopolymers* **2013**, *99*, 84.
[32] P. Laaksonen, M. Kainlauri, T. Laaksonen, A. Shchepetov, H. Jiang, J. Ahopelto, M. B. Linder, *Angew. Chem. Int. Ed.* **2010**, *49*, 4946.
[33] Z. Wang, Y. Wang, Y. Huang, S. Li, S. Feng, H. Xu, M. Qiao, *Carbon* **2010**, *48*, 2890.
[34] K. Kurppa, H. Jiang, G. R. Szilvay, A. G. Nasibulin, E. I. Kauppinen, M. B. Linder, *Angew. Chem. Int. Ed.* **2007**, *46*, 6446.
[35] J. Bayry, V. Aimanianda, J. I. Guijarro, M. Sunde, J.-P. Latgé, *PLoS Pathog.* **2012**, *8*, e1002700.
[36] X. Wang, H. Wang, Y. Huang, Z. Zhao, X. Qin, Y. Wang, Z. Miao, Q. Chen, M. Qiao, *Biosens. Bioelectron.* **2010**, *26*, 1104.
[37] M. P. Sarparanta, L. M. Bimbo, E. M. Mäkilä, J. J. Salonen, P. H. Laaksonen, A. M. K. Helariutta, M. B. Linder, J. T. Hirvonen, T. J. Laaksonen, H. A. Santos, A. J. Airaksinen, *Biomaterials* **2012**, *33*, 3353.
[38] H. K. Valo, P. H. Laaksonen, L. J. Peltonen, M. B. Linder, J. T. Hirvonen, T. J. Laaksonen, *ACS Nano* **2010**, *4*, 1750.
[39] M. B. Linder, G. R. Szilvay, T. Nakari-Setälä, M. E. Penttilä, *FEMS Microbiol. Rev.* **2005**, *29*, 877.
[40] H. J. Hektor, K. Scholtmeijer, *Curr. Opin. Biotechnol.* **2005**, *16*, 434.
[41] V. Aimanianda, J. Bayry, S. Bozza, O. Kniemeyer, K. Perruccio, S. R. Elluru, C. Clavaud, S. Paris, A. A. Brakhage, S. V Kaveri, L. Romani, J.-P. Latgé, *Nature* **2009**, *460*, 1117.
[42] L. De Stefano, I. Rea, E. De Tommasi, I. Rendina, L. Rotiroti, M. Giocondo, S. Longobardi, A. Armenante, P. Giardina, *Eur. Phys. J. E. Soft Matter* **2009**, *30*, 181.
[43] A. Zykwinska, M. Pihet, S. Radji, J.-P. Bouchara, S. Cuenot, *Biochim. Biophys. Acta* **2014**, *1844*, 1137.
[44] A. Zykwinska, T. Guillemette, J.-P. Bouchara, S. Cuenot, *Biochim. Biophys. Acta* **2014**, *1844*, 1231.
[45] I. Macindoe, A. H. Kwan, Q. Ren, V. K. Morris, W. Yang, J. P. Mackay, M. Sunde, *Proc. Natl. Acad. Sci. U.S.A.* **2012**, *109*, E804.
[46] V. K. Morris, Q. Ren, I. Macindoe, A. H. Kwan, N. Byrne, M. Sunde, *J. Biol. Chem.* **2011**, *286*, 15955.

[47] I. M. Tucker, J. T. Petkov, J. Penfold, R. K. Thomas, P. Li, A. R. Cox, N. Hedges, J. R. P. Webster, *J. Phys. Chem. B* **2014**, *118*, 4867.
[48] S. Longobardi, D. Picone, C. Ercole, R. Spadaccini, L. De Stefano, I. Rea, P. Giardina, *Biomacromolecules* **2012**, *13*, 743.
[49] A. Armenante, S. Longobardi, I. Rea, L. De Stefano, M. Giocondo, A. Silipo, A. Molinaro, P. Giardina, *Glycobiology* **2010**, *20*, 594.
[50] S. Houmadi, R. D. Rodriguez, S. Longobardi, P. Giardina, M. C. Fauré, M. Giocondo, E. Lacaze, *Langmuir* **2012**, *28*, 2551.
[51] L. De Stefano, I. Rea, P. Giardina, A. Armenante, I. Rendina, *Adv. Mater.* **2008**, *20*, 1529.
[52] I. Rea, P. Giardina, S. Longobardi, F. Porro, V. Casuscelli, I. Rendina, L. De Stefano, *J. R. Soc. Interface* **2012**, *9*, 2450.
[53] S. Longobardi, A. M. Gravagnuolo, R. Funari, B. Della Ventura, F. Pane, E. Galano, A. Amoresano, G. Marino, P. Giardina, *Anal. Bioanal. Chem.* **2014**, *407*, 487.
[54] L. De Stefano, I. Rea, A. Armenante, P. Giardina, M. Giocondo, I. Rendina, *Langmuir* **2007**, *23*, 7920.
[55] V. Georgakilas, M. Otyepka, A. B. Bourlinos, V. Chandra, N. Kim, K. C. Kemp, P. Hobza, R. Zboril, K. S. Kim, *Chem. Rev.* **2012**, *112*, 6156.
[56] K. Kostarelos, K. S. Novoselov, *Science* **2014**, *344*, 261.
[57] P. Wick, A. E. Louw-Gaume, M. Kucki, H. F. Krug, K. Kostarelos, B. Fadeel, K. A. Dawson, A. Salvati, E. Vázquez, L. Ballerini, M. Tretiach, F. Benfenati, E. Flahaut, L. Gauthier, M. Prato, A. Bianco, *Angew. Chemie Int. Ed.* **2014**, *53*, 7714.
[58] K. R. Paton, E. Varrla, C. Backes, R. J. Smith, U. Khan, A. O'Neill, C. Boland, M. Lotya, O. M. Istrate, P. King, T. Higgins, S. Barwich, P. May, P. Puczkarski, I. Ahmed, M. Moebius, H. Pettersson, E. Long, J. Coelho, S. E. O'Brien, E. K. McGuire, B. M. Sanchez, G. S. Duesberg, N. McEvoy, T. J. Pennycook, C. Downing, A. Crossley, V. Nicolosi, J. N. Coleman, *Nat. Mater.* **2014**, *13*, 624.
[59] E. Lurie-Luke, *Biotechnol. Adv.* **2014**, *32*, 1494.
[60] U. Khan, A. O'Neill, H. Porwal, P. May, K. Nawaz, J. N. Coleman, *Carbon* **2012**, *50*, 470.
[61] A. Bianco, *Angew. Chem. Int. Ed.* **2013**, *52*, 4986.
[62] Y. Ma, H. Shen, X. Tu, Z. Zhang, *Nanomedicine* **2014**, *9*, 1565.
[63] A. Bianco, H.-M. Cheng, T. Enoki, Y. Gogotsi, R. H. Hurt, N. Koratkar, T. Kyotani, M. Monthioux, C. R. Park, J. M. D. Tascon, J. Zhang, *Carbon* **2013**, *65*, 1.
[64] A. Eckmann, A. Felten, A. Mishchenko, L. Britnell, R. Krupke, K. S. Novoselov, C. Casiraghi, *Nano Lett.* **2012**, *12*, 3925.
[65] A. O'Neill, U. Khan, P. N. Nirmalraj, J. Boland, J. N. Coleman, *J. Phys. Chem. C* **2011**, *115*, 5422.
[66] U. Khan, A. O'Neill, M. Lotya, S. De, J. N. Coleman, *Small* **2010**, *6*, 864.